

Multi-step Effects in Subcoulomb Breakup

F.M. Nunes*

¹⁾*Universidade Fernando Pessoa, Praça 9 de Abril, 4200 Porto, Portugal*

²⁾*CENTRA, Instituto Superior Técnico, 1096 Lisboa-Codex, Portugal.*

I. J. Thompson

Department of Physics, University of Surrey, Guildford GU2 5XH, UK

(October 7, 2018)

Abstract

Following earlier one-step calculations, we explore the contributions of multi-step effects for the breakup of low energy ^8B on ^{58}Ni and ^{208}Pb within a coupled discretised continuum channels (CDCC) formalism. The Coulomb multi-step differential cross section is significantly reduced for all angles, the largest effect being the destructive interference of nuclear couplings. The nuclear peak, at around 80° in the one-step calculations for ^{58}Ni , virtually disappears.

24.10.Eq, 25.60.-t, 25.60.Gc, 27.20.+n

Typeset using REVTeX

*Email address: filomena@wotan.ist.utl.pt

I. INTRODUCTION

Coulomb dissociation has been proposed on many occasions [1,2] as a means of determining the interaction between fragments at low relative energies. This method is applicable even when the fragments are themselves radioactive and not easily produced as targets for direct scattering experiments. It was believed that at sufficiently forward angles, and/or at sufficiently low energies, the impact parameters for the breakup trajectory would be large enough for Coulomb mechanisms to dominate, and for first-order theories of Coulomb breakup to be adequate. The Coulomb dissociation method deduces the radiative capture cross section by measuring the reverse reaction, the dissociation of a projectile (the fused system) by the Coulomb field of a target.

The Coulomb dissociation method has been used to examine the breakup of ${}^8\text{B}$ at both high [3,4] and low [5] energies. Analyses have started with semiclassical theory [6], and have progressed to include the $E1/E2/M1$ contributions with correct experimental efficiencies [7], three-body kinematics in the final state [8], and most recently one-step nuclear and Coulomb contributions [9–11]. These last results, and those of ref. [12], showed that the nuclear and Coulomb form factors extend to considerably larger distances than the sum of the radii of the participating nuclei, because of the extended tail of the wave function of the last proton in ${}^8\text{B}$, and that there is strong Coulomb-nuclear destructive interference at intermediate radii. We are prompted, by the size of these effects, to examine the importance of *multi-step* contributions for both Coulomb and nuclear processes, taking into account the final state interactions which were previously omitted. These final-state interactions will couple together the different continuum states, and also describe the depletion of the elastic channel due to breakup. The depletion effect has been considered in some calculations [12], where only couplings between the bound state and continuum states were included. The contribution of ‘higher-order breakup’ has yet to be properly clarified, especially the role of continuum-to-continuum couplings.

Earlier treatments of multi-step effects for breakup have used either adiabatic [13] or semiclassical approximations [14,15], solved the scattering problem with time-dependent methods [16], tried CDCC solutions [17,18], or used Bremstrahlung integrals [19,20]. Estimates of second-order Coulomb and nuclear effects have also been calculated [21].

The earliest adiabatic approximation used the three-body wave functions of Amakawa et al. [22] within a prior-form breakup matrix element [13] for both nuclear and Coulomb mechanisms in the ${}^7\text{Li}$ breakup into $\alpha + t$, when incident on ${}^{208}\text{Pb}$ at 70 MeV. However, the best fit to the experimental cross sections was found when both Coulomb distortion and Coulomb breakup were omitted from the calculation. The breakup of ${}^6\text{Li}$ into $\alpha + d$, when incident on ${}^{208}\text{Pb}$ at 156 MeV, was later analysed [17] within the CDCC framework [18], and strong nuclear and Coulomb interference effects were found, even at forward angles. We follow a similar CDCC approach, but extend it to include, for the first time, dipole as well as quadrupole Coulomb mechanisms.

Recent investigations of the breakup of halo nuclei have prompted a revival of semiclassical treatments of breakup [14,15,23] where the continuum is discretised into an orthogonal set of basis functions. First-order and higher-order couplings can then be included when integrating along a semiclassical trajectory (Rutherford orbit at low energies, or straight lines at high energies). Simplified ground-state wave functions are often used, and collective

rather than semi-microscopic form factors calculated. We will see below that both of these approximations have to be reviewed when we consider the breakup of ${}^8\text{B}$ incident on ${}^{58}\text{Ni}$ at the sub-Coulomb energy of 26 MeV.

Another method, successfully used [16,24] to treat higher-order processes, is to follow the breakup reaction as a time-dependent process. Esbensen et al. [16] follow the time evolution of a ${}^7\text{Be}+p$ bound state by means of a TDHF propagator along a straight-line trajectory, and can calculate both Coulomb and nuclear contributions to breakup in a unitary manner. The results [16] show that the Coulomb higher-order dynamical processes cause a destructive E1/E2 interference, and a reduction of the dissociation probability.

Most recently, the adiabatic three-body wave functions have been used again [19,20] for Coulomb breakup, since in this case analytic solutions have been discovered both for the three-body wave functions [25] and for the post-form T -matrix integral of the breakup matrix element [19] in terms of a Bremstrahlung integral. Unfortunately, the method is not immediately applicable for ${}^8\text{B}$ breakup, since these analytic solutions only hold for neutral valence particles, and the adiabatic approximations are for high energy rather than for sub-Coulomb reactions.

We have been progressively improving our understanding of low energy breakup reactions [9–11], focusing in particular on the breakup of ${}^8\text{B}$ on ${}^{58}\text{Ni}$ measured by the Notre Dame group [5] at 26 MeV. The work presented here is an exploratory continuation of our previous investigations, and now, for the first time, a full multi-step quantum mechanical description is attempted, including all continuum couplings.

II. THEORY

A. Coupled Discretised Continuum Channels (CDCC)

When a projectile is described as a single particle outside a core, its state can be disturbed by the interaction with the target nucleus, as the tidal forces of the target act differentially on the particle and the core. If one separates the projectile-target interaction into $V_{ct}(\mathbf{R}_c)$, the interaction of the target nucleus with the core, and $V_{pt}(\mathbf{r}')$, the interaction of the target nucleus with the particle, then there is a mechanism for coupling ground and inelastic (continuum) states together. Nuclear and Coulomb components of V_{ct} and V_{pt} should be included on the same footing.

In order to describe the breakup of a projectile such as ${}^8\text{B}$, we could consider the inelastic excitations in the $p+{}^7\text{Be}$ system from the ground state $\phi_{gs}(r)$ to excited states in the continuum $u_{\ell sj,k}(r)$, for some momentum k and partial wave ℓ . The use of such single energy eigenstates, however, would result in calculations of the inelastic form factors which will not converge, as the continuum wave functions do not decay to zero as $r \rightarrow \infty$ sufficiently fast to be square integrable. One way [26,27] of dealing with this divergence is to take continuum states, not at a single energy, but averaged over a narrow range of energies, such that these ‘bin’ states *are* square integrable. We label these bin states by their wave-number limits $[k_1, k_2]$ and their angular momentum quantum numbers $(\ell s)j$. We use them in the coupled discretised continuum channels (CDCC) method [26,27].

Let \mathbf{R} be the coordinate from the target to the projectile and \mathbf{r} the internal coordinate of the projectile. The position coordinates of the projectile fragments with respect to the

target are

$$\mathbf{r}' = \mathbf{R} + \frac{A_p - 1}{A_p} \mathbf{r}$$

and

$$\mathbf{R}_c = \mathbf{R} - \frac{1}{A_p} \mathbf{r},$$

where the projectile has mass A_p .

The wave function for the three-body system of proton + ${}^7\text{Be}$ core + target is expanded as

$$\Psi_J^M(\mathbf{R}, \mathbf{r}) = \sum_{L\ell j, [k_1, k_2], M_L \mu} \phi_{\ell s j, [k_1, k_2]}^\mu(\mathbf{r}) \langle LM_L j \mu | JM \rangle i^L Y_L^{M_L}(\hat{\mathbf{R}}) \frac{1}{R} f_{L, \ell j [k_1, k_2], J}(R), \quad (1)$$

with

$$\phi_{\ell s j, [k_1, k_2]}^\mu(\mathbf{r}) = \frac{1}{r} \sum_{m\sigma} \langle \ell m s \sigma | j \mu \rangle Y_\ell^m(\hat{\mathbf{r}}) \chi_s^\sigma u_{\ell s j, [k_1, k_2]}(r), \quad (2)$$

where χ_s^σ is the proton's intrinsic state. The set $\{L, \ell, s, j, [k_1, k_2]\}$ will be abbreviated as α .

The radial wave functions $f_{L, \ell j [k_1, k_2], J}(R)$ satisfy the set of coupled equations

$$\left[-\frac{\hbar^2}{2\mu} \left(\frac{d^2}{dR^2} - \frac{L(L+1)}{R^2} \right) + \epsilon([k_1, k_2]) - E \right] f_{\alpha J}(R) + \sum_{\alpha'} i^{L'-L} V_{\alpha:\alpha'}^J(R) f_{\alpha' J}(R) = 0, \quad (3)$$

where $\epsilon([k_1, k_2])$ is the average energy of continuum bin $[k_1, k_2]$, (or $\epsilon < 0$ for the ground state). $V_{\alpha:\alpha'}^J(R)$ describes the coupling between the different relative motion states:

$$V_{\alpha:\alpha'}^J = \langle \phi_\alpha(\mathbf{r}) | V_{ct}(\mathbf{R}_c) + V_{pt}(\mathbf{r}') | \phi_{\alpha'}(\mathbf{r}) \rangle, \quad (4)$$

where $V_{ct}(\mathbf{R}_c)$ and $V_{pt}(\mathbf{r}')$ are again the total (nuclear and Coulomb) interactions between $c-t$ and $p-t$ systems respectively. In Eq.(4) radial integrations are done over r from zero to R_{bin} , a parameter to be chosen.

The coupled equations of Eq.(3) may be solved exactly [29] if they are not too numerous. Otherwise, iterative expansions are used starting with $f^{(-1)}(R) = 0$, and continuing as

$$\begin{aligned} & \left[-\frac{\hbar^2}{2\mu} \left(\frac{d^2}{dR^2} - \frac{L(L+1)}{R^2} \right) + V_{\alpha:\alpha}^J(R) + \epsilon([k_1, k_2]) - E \right] f_{\alpha J}^{(n)}(R) \\ & = \sum_{\alpha' \neq \alpha} i^{L'-L} V_{\alpha:\alpha'}^J(R) f_{\alpha' J}^{(n-1)}(R), \end{aligned} \quad (5)$$

for $n=0, 1, \dots$. The function $f^{(0)}(R)$ is thus the elastic channel, and the asymptotic S -matrix $S^{(n)}$ of the wave functions $f^{(n)}(R)$ gives the cross section for n^{th} -order DWBA. The $n=1$ first-order DWBA solutions are presented in the previous paper [11]. The multi-step DWBA results for large n will converge to the coupled-channels solution if the off-diagonal couplings are small. If they are large, the DWBA series diverges. Then the infinite series may be summed by the method of Padé approximants described below.

The bin wave functions are defined as

$$u_{\ell sj, [k_1, k_2]}(r) = \sqrt{\frac{2}{\pi N}} \int_{k_1}^{k_2} w(k) e^{-i\delta_k} u_{\ell sj, k}(r) dk, \quad (6)$$

with δ_k the scattering phase shift for $u_{\ell sj, k}(r)$, the single-energy scattering wave function in the chosen potential $V_{pc}^\ell(r)$ which may be ℓ -dependent. The normalisation constant is $N = \int_{k_1}^{k_2} |w(k)|^2 dk$ for the assumed weight function $w(k)$, here taken to be unity. These bin states are normalised $\langle u|u \rangle = 1$ once a sufficiently large maximum radius R_{bin} for r is taken. They are orthogonal to any bound states, and are orthogonal to other bin states if their energy ranges do not overlap. The phase factor $e^{-i\delta_k}$ ensures that they are all real valued for real potentials $V_{pc}^\ell(r)$.

The rms radius of a bin wave function increases as the bin width $k_2 - k_1$ decreases, approximately as $1/(k_2 - k_1)$, so large radial ranges are needed to include narrow bin states. If the maximum radius R_{bin} is not sufficiently large, then the bin wave functions $u_{[k_1, k_2]}$ will not accurately be normalised to unity by the factors given in equation (6). It is important however, to realise that the missing normalisation comes at large distances; the bin wave functions must not be artificially renormalised to unity, otherwise, for example, the correct Coulomb B(EK) distributions will not be obtained.

The couplings $V_{\alpha: \alpha'}^J(R)$ in Eq.(3) arise, as discussed above, from the interaction potentials of the projectile fragments with the target. Assuming that the potentials V_{ct} and V_{pt} are central, the Legendre multipole potentials can be formed as

$$\mathcal{V}_K(R, r) = \frac{1}{2} \int_{-1}^{+1} [V_{ct}(\mathbf{R}_c) + V_{pt}(\mathbf{r}')] P_K(x) dx, \quad (7)$$

where K is the multipole and $x = \hat{\mathbf{r}} \cdot \hat{\mathbf{R}}$ is the cosine of the angle between \mathbf{r} and \mathbf{R} . Since s is the (fixed) spin of the proton, a spectator, the coupling form factor between states $u_{\ell' [k_1, k_2]'}(r)$ and $u_{\ell [k_1, k_2]}(r)$ is then

$$\begin{aligned} V_{\alpha: \alpha'}^J(R) &= \sum_K (-1)^{j+j'-J-s} \hat{j} \hat{j}' \hat{\ell} \hat{\ell}' \hat{L} \hat{L}' (2K+1) W(jj'\ell\ell'; Ks) W(jj'LL'; KJ) \\ &\times \begin{pmatrix} K & \ell & \ell' \\ 0 & 0 & 0 \end{pmatrix} \begin{pmatrix} K & L & L' \\ 0 & 0 & 0 \end{pmatrix} \int_0^{R_{bin}} u_{\ell sj [k_1, k_2]}(r) \mathcal{V}_K(R, r) u_{\ell' sj' [k_1, k_2]'}(r) dr. \end{aligned} \quad (8)$$

From the S -matrices $S^{(n)}$ we calculate the double differential cross sections $d^2\sigma/d\Omega d\epsilon$, where Ω is the scattering angle of the centre of mass of the ${}^8\text{B}^*$ fragments p and c , and ϵ is the excitation energy within ${}^8\text{B}^*$. Usually we will plot the integrated angular distribution $d\sigma/d\Omega$ obtained after summation over all the bin energies $\epsilon([k_1, k_2])$. It will be possible [27,28] to obtain from the CDCC results the full multiple differential cross sections such as $d^3\sigma/d\Omega_p d\Omega_c dE_p$, and then, for example, any post-acceleration effects may be determined from the variation of the cross section with respect to the laboratory proton energy E_p . An approximate treatment is available [8,11] to calculate these fragment distributions using an isotropic assumption for the pc relativ motion, but this does not yet include the interference between the different final ℓ -states that is necessary [15] to give non-zero post-acceleration effects.

B. Padé acceleration

A given sequence $S^{(0)}, S^{(1)}, \dots$ of S-matrix elements that result from iterating the coupled equations can be regarded as the successive partial sums of the polynomial

$$f(\lambda) = S^{(0)} + (S^{(1)} - S^{(0)})\lambda + (S^{(2)} - S^{(1)})\lambda^2 + \dots \quad (9)$$

evaluated at $\lambda=1$. This polynomial will clearly converge for λ sufficiently small, but will necessarily diverge if the analytic continuation of the $f(\lambda)$ function has any pole or singularities inside the circle $|\lambda| < 1$ in the complex λ -plane. The problem that Padé approximants solve is that of finding a computable approximation to the analytic continuation of the $f(\lambda)$ function to $\lambda=1$. This is accomplished by finding a rational approximation

$$P_{[N,M]}(\lambda) = \frac{p_0 + p_1\lambda + p_2\lambda^2 + \dots + p_N\lambda^N}{1 + q_1\lambda + q_2\lambda^2 + \dots + q_M\lambda^M} \quad (10)$$

which agrees with the $f(\lambda)$ function in the region where the latter does converge, as tested by matching the coefficients in the polynomial expansion of $P_{[N,M]}(\lambda)$ up to and including the coefficient of λ^n for $n = N + M$.

There are many different ways [30] of evaluating the coefficients p_i, q_j , but for the present problem we can use Wynn's ϵ -algorithm [31,32], which is a method of evaluating the upper right half of the Padé table at $\lambda=1$ directly in terms of the original sequence $S^{(0)}, S^{(1)}, \dots$. Experience has shown that for typical sequences the most accurate Padé approximants are those near the diagonal of the Padé table. We use $\overline{S^{(n)}} \equiv P_{[N,M]}(1)$ for $N = [(n+1)/2]$ and $M = [n/2]$ in calculating the Padé-resummed cross sections.

When accelerating a *vector* of S-matrix elements $\mathbf{S}^{(n)}$, with a component for each coupled channel α , then it is important to accelerate the vector as a whole. Wynn [33] pointed out that this can be done using the Samuelson inverse

$$\mathbf{x}^{-1} = (\mathbf{x} \cdot \mathbf{x}^*)^{-1} \mathbf{x}^* \quad (11)$$

where \mathbf{x}^* is the complex conjugate of \mathbf{x} .

III. RESULTS

The multi-step DWBA calculations presented here were calculated using FRESKO [29]. We use a continuum breakup subspace sufficient to reproduce what we believe to be the principal channels. For the distorted waves of the projectile-target wave function, radii up to $R_{coup} = 300$ fm and partial waves up to $L_{max} = 600$ were included to ensure full convergence of the individual angular distributions. These limits give, by semiclassical considerations, cutoffs for Coulomb excitations below 2.0° from our L_{max} , and below 1.7° from our R_{coup} value. We have examined the convergence with respect to R_{bin} . For the case we are interested in, the differential cross section remains unaltered as long as $R_{bin} \geq 50$ fm. Thus, each energy bin (Eq.6 and Eq.8) is calculated using $R_{bin} = 50$ fm.

It is essential for physical completeness that our calculations include monopole, dipole and quadrupole contributions for both nuclear and Coulomb mechanisms. However, they do

not include $M1$ transitions. At the extreme nonrelativistic velocities of interest here, these are predicted (see for instance [5]) to be insignificant.

In Fig.(1) we show the energy distribution of the cross section obtained within a 1-step calculation, using the ${}^8\text{B}$ model from Esbensen [16]. We keep the same $p+{}^7\text{Be}$ potential (that defined for the ground state) for all partial waves of relative motion. For scattering from ${}^{58}\text{Ni}$ we use the same optical potentials [34,35] as in [9]. The cross section is plotted as a histogram to illustrate the continuum discretisation that we have used to define the energy bins included in all calculations. These results show that transitions from the ${}^7\text{Be}$ - $p_{3/2}$ ground state to s,p,d, and f-wave continuum states up to 3 MeV should be taken into account, even though one can expect f-waves to offer only a small correction to the overall result. A finer discretisation of p, d and f waves would be desirable, but the present (70 bin) calculation is already at the limit of our computational capacity.

We first calculate multi-step effects by iterating the coupled equations beyond the first-order DWBA. We find that even the second-order DWBA diverges rapidly, especially for low partial waves (small impact parameters), and does not give sensible results beyond 30° (dashed line with circles in Fig. 2). In order, therefore, to present some indications on what may be deduced from the successive Born terms, we will present the results when resumming the expansion using the method of Padé acceleration (see section II B) for successive numbers of steps n . We will use for cross sections the Padé approximants the $\overline{S^{(n)}}$ rather than the original $S^{(n)}$ matrices. Given the nature of our expansion, it is not possible to directly compare 2nd and 3rd order effects with those obtained using the pure conventional DWBA expansion.

Fig.(2) shows the 1-step, 2-step, 3-step, 6-step and 20-step breakup results using Padé acceleration. The rate of convergence of this resummed expansion is encouraging, contrary to that of the original Born series which diverges strongly immediately at 2nd order. In addition, we show in figs.(3) and (4) the different rate of convergence for the ${}^8\text{B}$ breakup into s and p continuum states considering the Coulomb and nuclear interactions separately. In all the cases we have studied, the Padé convergence is non monotonic. If one includes 1-step and 2-step processes only, the differential cross section is underestimated. Introducing 3-step corrections overestimates the cross section. From our results we conclude that for the breakup of low energy ${}^8\text{B}$ on ${}^{58}\text{Ni}$, contributions up to at least 9th order in the Padé expansion should be included.

Still in Fig.(2) we present the results obtained for the full coupled channel calculation taking into account s-wave and p-wave bins. We find that processes beyond 20-step do not contribute to the cross section. For this reduced bin subspace (42 bins) it is possible to perform the full coupled channel calculation (light solid curve in Fig.2). It is reassuring to find that our results using the multi-step expansion with Padé acceleration converge to the correct full CDCC results. In the larger bin subspaces it is extremely hard to perform the full CDCC calculation and thus we will rely on the multi-step expansion with Padé acceleration.

Including multi-step effects, the Coulomb differential cross section is hardly modified up to $\theta \simeq 10^\circ$. The peak at $\theta \simeq 20^\circ$ is shifted to slightly smaller angles with higher order processes and its magnitude is reduced by $\simeq 10\%$ (see Fig.3).

The most striking result of our work is clearly the destructive interference caused by the nuclear multi-step processes. The nuclear peak is shifted to lower angles (from $\theta \simeq 80^\circ$ for 1-step calculations to $\theta \simeq 40^\circ$ for the CDCC calculations) and suffers a reduction to $\frac{1}{6}$ of

its peak value. We do not expect measurements of the breakup differential cross section at larger angles to provide a good handle for the optical potentials as one could deduce from the 1-step results presented in our earlier work [9]. The previously observed strong nuclear peak is practically washed away by multi-step effects.

We point out that, as in the 1-step calculations of [9], the total differential cross section does not correspond to the sum of Coulomb and nuclear contributions calculated separately. This can be seen in Fig.(5) where the sum of the Coulomb and nuclear cross sections for the CDCC calculation is compared with the CDCC cross section when Coulomb and nuclear are treated in the same footing. As in [9,11] there is a wide range of angles where the Coulomb-nuclear interference effects cannot be neglected.

So far we have included all possible couplings within the subspace considered. However it is useful to identify the relative importance of the continuum-continuum couplings as compared to the couplings to and from the ground state. In Fig.(6) we show the results of calculating the full multi-step breakup into s and p bin-states, including continuum-continuum couplings (dark lines) and excluding them (light lines). As can be seen, the continuum-continuum couplings are responsible for the significant cross section reduction, which are not merely due to depletion of flux from the elastic channel. The reduction is still obtained in calculations (not shown) with E2 couplings acting to only first order, but not in those with E1 couplings only to first order. This indicates that the reduction is caused by multistep E1 processes interfering with low-order E2 transitions, a process similar to that seen in ref. [16].

In order to elucidate the different ${}^8\text{B}$ partial wave contributions, we show in Fig.(7) the differential cross section obtained for the full multi-step breakup including: s (dotted), s+p (short-dashed), s+p+d (long-dashed) and s+p+d+f (dot-dashed) bin states. A good description of the physics can be obtained without d and f-waves, although if one wishes to extract quantitative results these should be included together with a finer energy-bin grid.

One of the main motivations of ${}^8\text{B}$ breakup experiments is astrophysical, to determine the S_{17} at low relative energies. It is thus important to disentangle the dependence on the ${}^8\text{B}$ structure model. This was the main concern of our earlier work [10]. In Fig.(8) we present a comparison of differential cross sections for two ${}^8\text{B}$ models: that of Kim [36], and our initial model, from Esbensen [16]. The latter has a smaller radius in order to reproduce $S_{17} \simeq 17$ eV b. The difference between the multi-step results using the two structure models is generally similar to the difference in the 1-step results: there is an overall normalisation due to the size of the projectile but no significant shape change. For this particular case, the Kim model produces a 30% increase in the total differential cross section.

The Notre Dame group is considering repeating their experiment [5] with a heavier target at the same beam energy, hoping then the $E2$ contribution will be easier to extract. We have therefore performed one and multistep calculations for a ${}^{208}\text{Pb}$ target, for all combinations of nuclear and Coulomb mechanisms (see Fig.9). We have taken the ${}^{208}\text{Pb}$ - proton optical interaction from [37]. For the optical potential between ${}^7\text{Be}$ and ${}^{208}\text{Pb}$ we have used a heavy-ion global parameterisation [38]. We have checked that the differential cross section is not sensitive to variations on the core-target optical parameters, and thus we expect these results to give a good indication of the physical effects. In order to have quantitative results, measurements of the elastic scattering of ${}^7\text{Be}$ (or a nucleus in the same mass/charge region) on ${}^{208}\text{Pb}$ at these low energies would be necessary.

Our results show that the nuclear contribution is zero up to 50° and becomes important only at backward angles. Given these results, it should be possible to extract information on the magnitude of the electromagnetic components, as long as the detectors are placed at smaller angles. One should keep in mind that the multi-step processes reduce the Coulomb peak and alter its shape.

Similarly to what was found for ^{58}Ni and 1-step DWBA, for a ^{208}Pb target there are interference effects that do not allow a simple subtraction of the E2 component, as one would wish to obtain the S_{17} . In Fig.(10) we show the results for the CDCC calculations for the different electric components together with the full calculation. One can clearly see a destructive interference between E1 and E2 components. It may be possible to disentangle these components, but the result will inevitably be model dependent.

IV. CONCLUSIONS

Multistep calculations of low energy ^8B breakup on ^{58}Ni and ^{208}Pb , including all relevant couplings, have been performed for the first time. We have found it necessary to treat nuclear and Coulomb potentials on the same footing, since there is considerable interference between these mechanisms. Our calculations use the CDCC method, with Padé approximants to resum the Born series for the S-matrix. Exact coupled-channel calculations, possible in a reduced subspace, verify that this Padé resummation converges to the full coupled channel result. We compare our results with the one-step prior-form DWBA cross sections reported previously [9,11].

The multi-step effects are very strong, producing significant reductions of the cross section compared with those from first order theory. For Coulomb breakup we see pronounced interference effects for all angles at and beyond the peak position, while multi-step effects are much stronger for the nuclear part, so that, for the ^{58}Ni target, the nuclear peak resulting from the 1-step calculations virtually disappears. The prior-form DWBA thus overestimates the nuclear breakup probabilities at our sub-Coulomb incident energy. The multi-step reduction is principally due to the continuum-continuum couplings, not just to depletion of the elastic channel, and this indicates that the projectile undergoes considerable dynamical distortion and recombination during the reaction. The dominant qualitative changes caused by the multi-step effects are seen when including only s and p wave continuum bins, but d and f waves must be included for quantitative results.

The results for two different ^8B structure models show that the multi-step effects depend on the size of the projectile, and are not sensitive to other details of the ^8B g.s. wave function. With a ^{208}Pb target, the nuclear contribution is only significant for backward angles. Multi-step effects reduce the cross section and change the shape slightly. According to our results, for the extraction of the E2 component this experiment seems more promising than that with the lighter target, although care should be taken to account for the strong destructive Coulomb-Coulomb interference.

ACKNOWLEDGMENTS

We thank Jeff Tostevin for helpful discussions and comments. We would like to express our gratitude to Eduardo Lopes for helping out with many computational difficulties. UK support from the EPSRC grant GR/J/95867 and Portuguese support from JNICT PRAXIS/PCEX/P/FIS/4/96 are acknowledged. One of the authors, F. Nunes, was supported by JNICT BIC 1481.

REFERENCES

- [1] A.C. Shotter, V. Rapp, T. Davinson, D. Branford, N.E. Sanderson and M.A. Nagarajan, Phys. Rev. Letts. **53** (1984) 1539
- [2] G. Baur and H. Rebel, J. Phys. G **20** (1994) 1
- [3] T. Motobayashi et al., Phys. Rev. Letts. **73** (1994) 2680
- [4] T. Kikuchi et al., Phys. Letts. **B391** (1997) 261
- [5] Johannes von Schwarzenberg et al., Phys. Rev. **C53** (1996) R2598
- [6] K. Alder and A. Winther, *Electromagnetic Excitation*, (North Holland, Amsterdam, 1975)
- [7] R. Shyam, I.J. Thompson and A.K. Dutt-Majumder, Phys. Lett.B **371** (1996) 1
- [8] R. Shyam and I.J. Thompson, Phys. Lett.B **415** (1997) 315
- [9] F.M. Nunes and I.J. Thompson, Phys. Rev. **C57** (1998) R2818
- [10] F. M. Nunes, R. Shyam, I.J. Thompson, J. Phys. **G 24** (1998) 1575
- [11] R. Shyam and I.J. Thompson, submitted to Phys. Rev. C
- [12] C.H. Dasso, S.M. Lenzi and A. Vitturi, Nucl. Phys. **A639** (1998) 635
- [13] I.J. Thompson and M.A. Nagarajan, Phys. Lett. **123B** (1983) 379
- [14] C. Bertulani and L.F. Canto, Nucl. Phys. **A539** (1992) 163
- [15] A. Romanelli, L.F. Canto, R. Donangelo, P. Lotti, Nucl. Phys. **A588** (1995) 71c
- [16] H. Esbensen and G. Bertsch, Nucl. Phys. **A600** (1996) 37
- [17] Y. Hirabayashi and Y. Sakuragi, Phys. Rev. Lett. **69** (1992) 1892
- [18] Y. Sakuragi, M. Yahiro and M. Kamimura, Prog. Theo. Phys. Suppl. **89** (1986) 136
- [19] J.A. Tostevin et al, Phys. Letts. **B424** (1998) 219
- [20] J.A. Tostevin, S. Rugmai and R.C. Johnson, Phys. Rev. **C57** (1998) 3225
- [21] S. Typel and G. Baur, Nucl. Phys. **A573** (1994) 486; S. Typel, H.H. Wolter and G. Baur, Nucl. Phys. **A613** (1997) 147
- [22] H. Amakawa, S. Yamaji, A. Mori and K. Yazaki, Phys. Letts. **82B** (1979) 13
- [23] C. Bertulani, L.F. Canto and M.S. Hussein, Phys. Letts. **B353** (1995) 413
- [24] T. Kido, K. Yabana, and Y. Suzuki, Phys. Rev. C **50** (1994) R1276; Phys. Rev. C **53** (1996) 2296
- [25] R.C. Johnson, J.S. Al-Khalili and J.A. Tostevin, Phys. Rev. Letts. **79** (1997) 2771
- [26] G.H. Rawitscher, Phys. Rev. **C9** (1974) 2210, **C11** (1975) 1152, Nucl. Phys. **A241** (1975) 365; M. Yahiro and M. Kamimura, Prog. Theor. Phys. **65** (1981) 2046, **65** (1981) 2051.
- [27] Y. Sakuragi, M. Yahiro and M. Kamimura, Prog. Theor. Phys. Suppl. **89** (1986) 136.
- [28] Y. Iseri, M. Yahiro and M. Kamimura, Prog. Theor. Phys. Suppl. **89** (1986) 84.
- [29] I.J. Thompson, Computer Physics Reports, **7** (1988) 167
- [30] P.R. Graves-Morris, *Padé Approximants*, Institute of Physics, London and Bristol, 1973
- [31] P. Wynn, Numer. Math. **8** (1966) 264
- [32] A. Genz, p 112 in [30].
- [33] P. Wynn, Math. Comput. **16** (1961) 23
- [34] Z. Moroz et al., Nucl. Phys. **A 381** (1982) 294
- [35] F.D. Becchetti and G.W. Greenlees, Phys. Rev. **182** (1969) 1190
- [36] K.H. Kim, M.H. Park and B.T. Kim, Phys. Rev. **C53** (1987) 363
- [37] W. Makofske, G.W. Greenlees, H.S. Liers and G.J. Pyle, Phys. Rev. **C 5** (1972) 780
- [38] Ricardo Broglia and Aage Winther, *Heavy Ion Reactions*, Vol I, Addison-Wesley

FIGURES

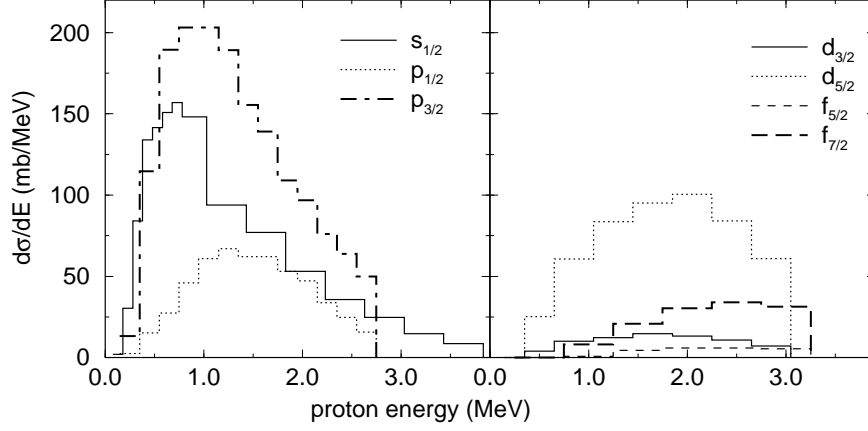


FIG. 1. Energy distribution of s, p, d and f partial wave bins.

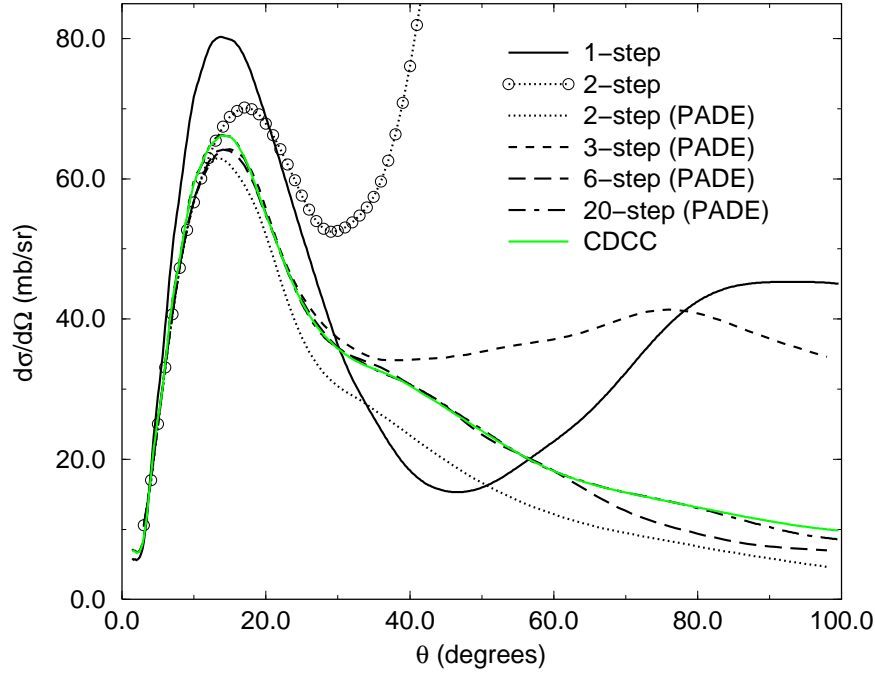


FIG. 2. The differential cross section obtained for multi-step breakup of ${}^8\text{B}$ into s and p-wave bins, including both Coulomb and nuclear effects: the full CDCC calculation, the 1-step and 2-step DWBA, and higher order calculations using Padé acceleration.

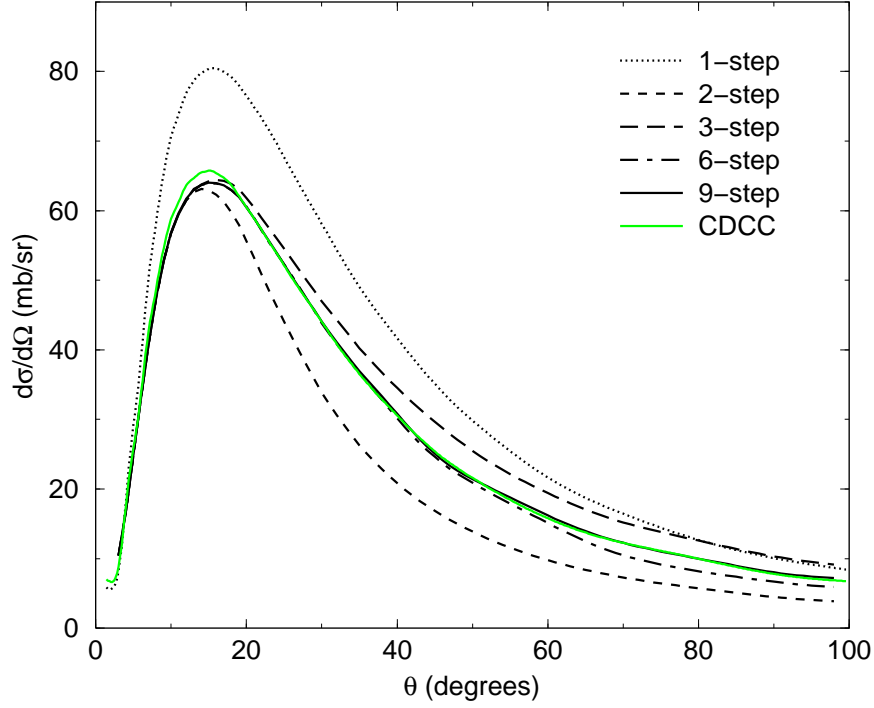


FIG. 3. The differential cross section obtained for the multi-step Coulomb breakup of ${}^8\text{B}$ into s and p-wave bins using Padé acceleration.

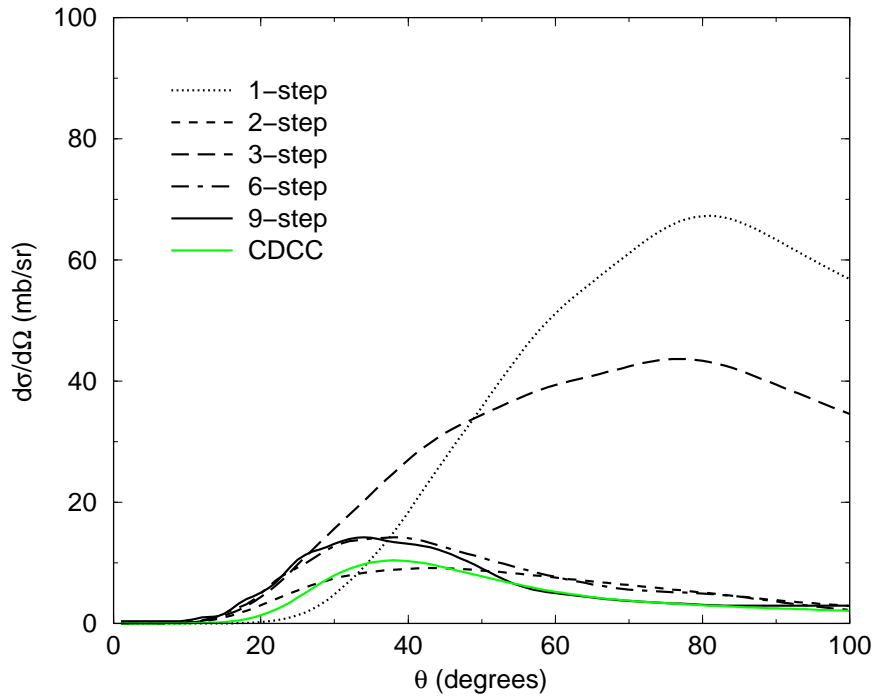


FIG. 4. The differential cross section obtained for the multi-step nuclear breakup of ${}^8\text{B}$ into s and p-wave bins, using Padé acceleration.

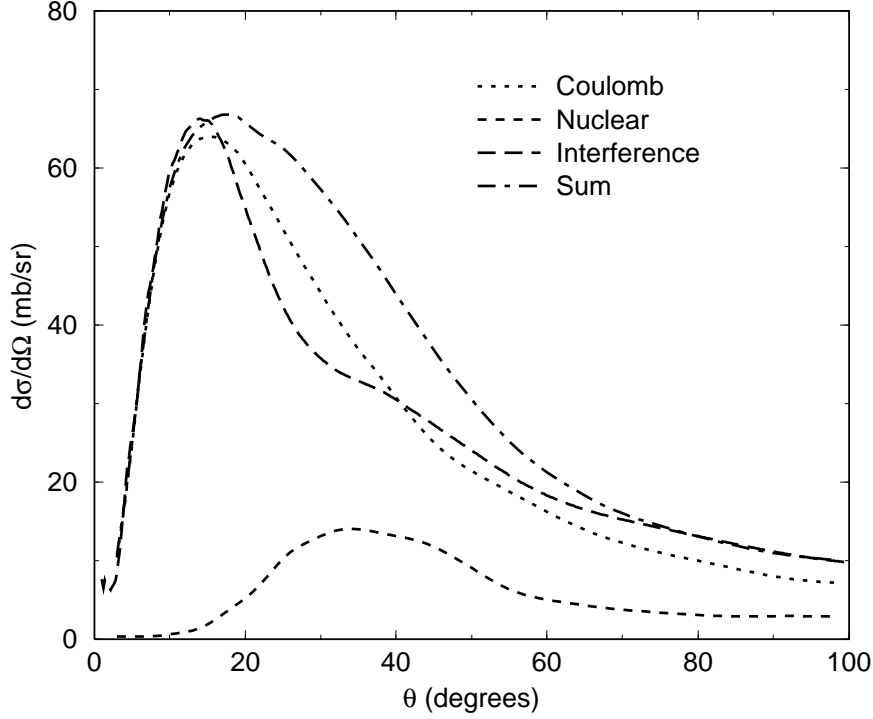


FIG. 5. The CDCC differential cross section obtained for the breakup of ${}^8\text{B}$ into s-wave and p-wave bins: comparison of the Coulomb and nuclear summed cross section with the calculation that includes nuclear-Coulomb interference.

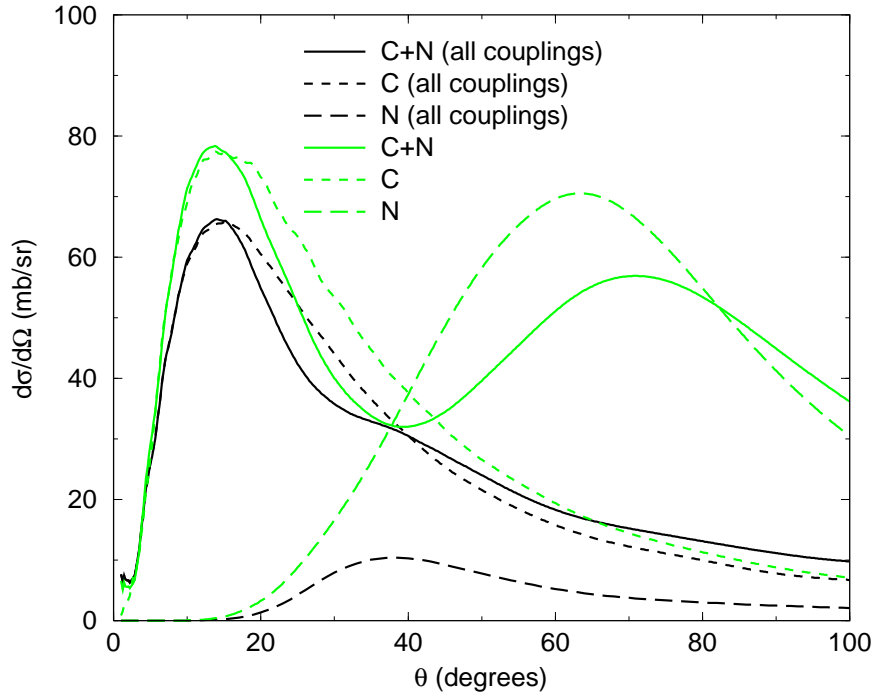


FIG. 6. Comparing the CDCC differential cross section when no continuum-continuum couplings are included in the calculation to the full calculation (this calculation includes s and p waves only).

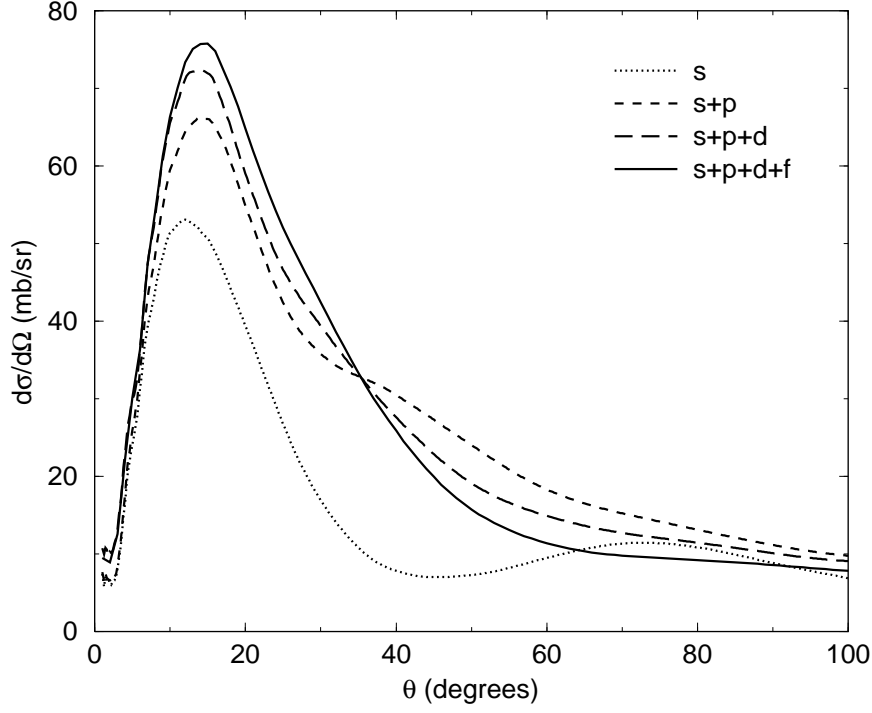


FIG. 7. Cumulative ^8B partial wave contributions to the CDCC differential cross section for Coulomb plus nuclear breakup to the $l=0,1,2$ and 3 channels.

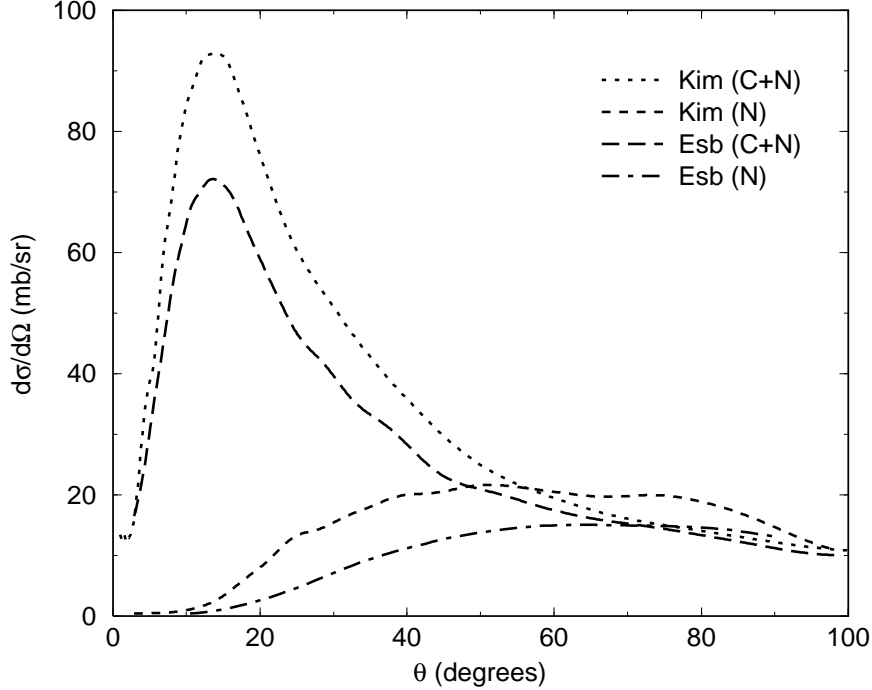


FIG. 8. Sensitivity to the ^8B structure model: the CDCC differential cross section including all but f-wave bins.

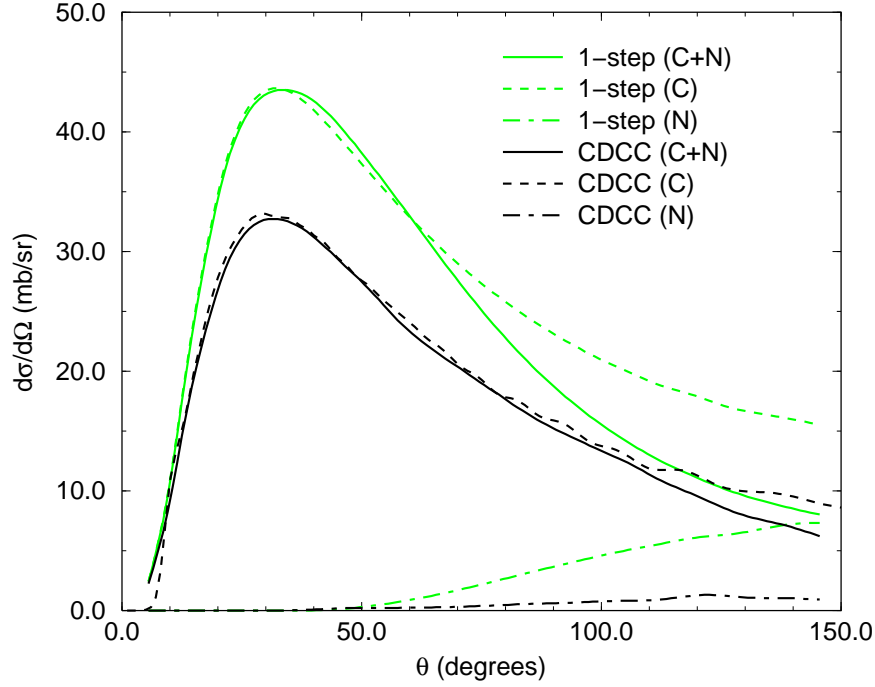


FIG. 9. Comparing the 1-step and CDCC differential cross section for ${}^8\text{B}$ breakup on ${}^{208}\text{Pb}$, including all but f-wave bins.

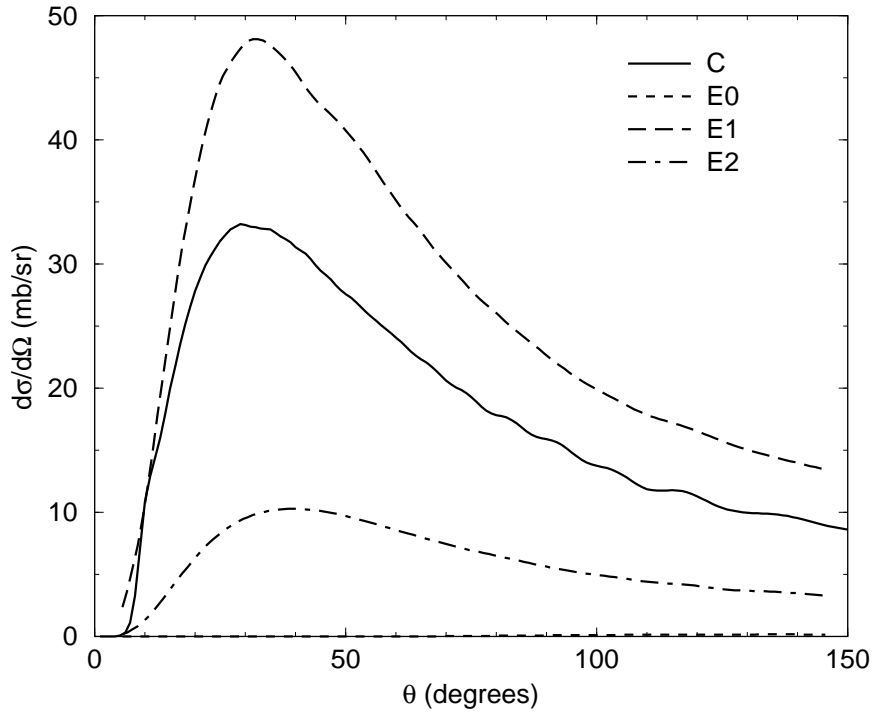


FIG. 10. Comparing the CDCC effects of only E0, only E1, and only E2 with the full Coulomb differential cross section for ${}^8\text{B}$ Coulomb breakup on ${}^{208}\text{Pb}$, including all but f-wave bins.